Title

Photopatternable and photoactive hydrogel for on-demand generation of hydrogen peroxide in cell culture

Journal

Biomaterials, 35(5)

ISSN

0142-9612

Authors

Garland, Shaun P

Wang, Royal Y

Raghunathan, Vijay Krishna

et al.

Publication Date

2014-02-01

DOI

10.1016/j.biomaterials.2013.11.030

Peer reviewed

Published in final edited form as:
Biomaterials. 2014 February ; 35(5): 1762–1770. doi:10.1016/j.biomaterials.2013.11.030.

Photopatternable and Photoactive Hydrogel for On-demand Generation of Hydrogen Peroxide in Cell Culture

Shaun P. Garland[a], **Royal Y. Wang**[a], **Vijay Krishna Raghunathan**[b], **Kit S. Lam**[c], **Christopher J. Murphy**[b,d], **Paul Russell**[b], **Gang Sun**[e], and **Tingrui Pan**[a,*]

[a]Micro-Nano Innovations (MiNI) Laboratory, Department of Biomedical Engineering, University of California, Davis, Davis, CA 95616 (USA)

[b]Department of Surgical & Radiological Sciences, School of Veterinary Medicine, University of California, Davis, Davis, CA 95616 (USA)

[c]Department of Biochemistry and Molecular Medicine, University of California, Davis, Davis, CA 95616 (USA)

[d]Department of Ophthalmology & Vision Sciences, School of Medicine, University of California, Davis, Davis, CA 95616 (USA)

[e]Division of Textiles and Clothing, University of California, Davis, Davis, CA 95616 (USA)

Abstract

Oxidative stress, largely mediated by reactive oxygen species (ROS), is a nearly ubiquitous component in complex biological processes such as aging and disease. Optimal *in vitro* methods used in elucidating disease mechanisms would deliver of low levels of hydrogen peroxide, emulating the *in vivo* pathological state, but current methods are limited by kinetic stability or accurate measurement of the dose administered. Here we present an *in vitro* platform that exploits anthraquinone catalysts for the photocatalytic production of hydrogen peroxide. This system can be dynamically tuned to provide constant generation of hydrogen peroxide at a desired physiologic rate over at least 14 days and is described using a kinetic model. Material characterization and stability is discussed along with a proof-of-concept *in vitro* study that assessed the viability of cells as they were oxidatively challenged over 24 h at different ROS generation rates.

Keywords

oxidative stress; hydrogen peroxide; anthraquinone; ROS

*Telephone: +1 530 754 9508; tingrui@ucdavis.edu.

1. Introduction

Reactive oxygen species (ROS) play a significant role in a wide range of biological and pathophysiological processes, including aging [1-4], signaling [5, 6], immune reactions [7], cancer development [5, 8], wound healing [9], and serve as a marker for numerous diseases [2, 10-13]. Mechanistic studies aimed at determining the role of ROS in disease states are difficult to perform *in vivo* as transgenic animal models missing critical antioxidant pathways exhibit dysfunction across the whole organism [14], and as a result, is no longer representative of the particular disease state under investigation. Because of this, the biological impact of oxidative stress is predominantly studied using *in vitro* methodologies, typically by acute bolus introductions of hydrogen peroxide (H_2O_2) and, less frequently, introduction superoxide salts into cell culture media [15]. While simple and convenient to perform, the intrinsic problems of this method are that supraphysiological doses of H_2O_2 are used (100-1000 μM) and the concentration decays rapidly over the course of a few hours [16] which is inconsistent with physiological conditions where submicromolar levels of H_2O_2 persist indefinitely [17]. Experiments performed by presenting a continuous oxidative profile that better represent physiological conditions tend to produce drastically different outcomes when compared to acute/bolus doses [18, 19] and are thought to be more biologically relevant. This was demonstrated during investigations into the molecular mechanisms of oxidative stress induced apoptosis, which required continuous oxidative challenge [20, 21]. Therefore generation of low levels of continuous oxidative stress is critical for enabling investigations that model disease processes and evaluate potential treatments *in vitro*.

Although continuous dosage techniques are physiologically more relevant for *in vitro* models of chronic diseases, the development of techniques to perform such experiments have received limited attention. Current methods that offer continuous delivery of H_2O_2 or superoxides include enzymatic systems (glucose oxidase [21-23] and xanthine oxidase [22]) and hyperoxic chambers [15, 24]_ENREF_24. These existing modalities suffer from a combination of issues associated with (a) undesirable variability in early *vs* steady state kinetics [21-23], (b) accumulation of counter-reactive by-products (e.g., glucono-δ-lactone and uric acid) [15], (c) limited tunability of the oxidative profile, (d) poor estimation of dose, and (e) reproducibility. Thus, there is a pressing need for a stable, tunable ROS generator that is compatible with the cell culture environment and yields a predictable dosage.

Anthraquinones (AQ) are photoactive compounds that undergo a photoreduction cycle to catalytically generate H_2O_2 upon exposure to UV and near-UV light [25, 26]_ENREF_26. The photoreductive property of AQs and their derivatives have been exploited to photograft DNA oligonucleotides [27] and polymers [28] to a variety of substrates. They have also been impregnated into textiles [29, 30] or chemically grafted onto surfaces [31, 32], polymers [33], and hydrogels [34] for generating H_2O_2 and creating light-powered antimicrobial surfaces. These properties suggest that AQs may make suitable *de novo* ROS generators for oxidative challenge studies.

Here we report a photoactive hydrogel-based material containing covalently bound AQ moieties that provide highly controllable long-term generation of H_2O_2 upon exposure to visible light. The kinetics and long-term stability of ROS generation are characterized under different AQ concentrations and activating light intensities. Furthermore, the physical properties are investigated and demonstrate covalent bonding of the AQs within hydrogel system. Lastly we employ this material as an *in vitro* continuous, tunable H_2O_2 generator and demonstrate its utility in a 'proof of concept' oxidative stress experiment.

2. Materials and Methods

2.1. Materials

Hydrogen peroxide (30%), 3-(4,5-Dimethyl-2-thiazolyl)-2,5-diphenyl-2H-tetrazolium bromide (MTT, >97.5%, cell culture grade), phosphate buffered saline (PBS), sodium 9,10-anthraquinone-2,6-disulfonate (2,6-AQS, >98%), poly(ethylene glycol) diacrylate (PEG-DA, mw 700 g/mol), xylenol orange tretrasodium salt (ACS grade), sorbitol (98%), ammonium iron(II) sulfate hexahydrate ($(NH_4)_2Fe(SO_4)_2$, 99%), and N,N,N',N'-Tetramethylethylenediamine (TEMED) were purchased from Sigma-Aldrich (St. Louis, MO). Hydrochloric acid (HCl, 12M), sulfuric acid (H_2SO_4, 96%) sodium chloride (NaCl, ACS grade), dibasic sodium phosphate (99%), HEPES (99%), dimethyl sulfoxide (DMSO, 99.7%), and ammonium persulfate (APS) were obtained from Fisher. Calcein-AM and ethidium homodimer-1 were purchased from Molecular Probes as a LIVE/DEAD viability kit and amplex red was from Life Technologies. Horse radish peroxidase (HRP, 250 U/mg) was obtained from MP Biomedicals (Solon, OH). Staining buffer was prepared with 150 mM NaCl, 2 mM Na_2HPO_4, 50 mM HEPES, and 2.5 mM $CaCl_2$ (96%, Acros) in DI water.

2.2. Synthesis and Fabrication

A stock solution of 4.0 mg/mL 2,6-AQS was prepared in DI water and acidified to pH 2 by HCl to increase solubility. The solution was protected from light and allowed several hours to fully dissolve. Prepolymer solutions were prepared by mixing equal volume PEG-DA with aqueous solution containing 0.5, 1, 2, or 4 mg/mL 2,6-AQS from the stock solution. Bulk hydrogels were photopolymerized in Ø15 × 1.5 mm disks with a low intensity 5 mW/cm^2 @ 365 nm UVA light at a dose of 150 mJ/cm^2. Afterwards, the hydrogels were allowed to stand for 20 min and subsequently swollen and extracted with PBS overnight. For photolithographically patterned hydrogels, 1-4 μL droplets of a prepolymer solution containing a 4 mg/mL 2,6-AQS aqueous component were placed on a chrome-glass photomask and sandwiched with an acrylated glass coverslip that had been treated with 3-acryloxypropyltrichlorosilane (Gelest) (silanization details in Supplemental Information). A collimated UV light source with a peak intensity at 365 nm of 25 mW/cm^2 was used to expose the patterns for 0.5 – 2 s. The patterns were developed with ethanol and gently dried with compressed air. For fluorescent ROS detection, photopatterned ROS hydrogel structures were backfilled with a prepolymer solution containing 10% HRP solution (10 mg/mL) and 90% PEG-DA [39], with 1% v/v of APS (50 mg/mL) and TEMED added to initiate crosslinking, and left to stand covered with a cover slip for 20 min. A 50 μM solution of amplex red in PBS was placed over the micropatterned hydrogel and exposed to UV light for 5 minutes and subsequently fluorescently imaged.

2.3. Material characterization

Swollen gels were punched to 10mm and placed in a 48-well plate (Costar) with 1 mL of PBS. To initiate photoreduction and stimulate the generation of hydrogen peroxide, the hydrogels were exposed to an array of 8 × 9 LEDs (5 mm, Bivar) with a peak intensity wavelength of 405 nm. For the long term stability study, hydrogels in triplicates formed with 0.5-4 mg/mL aqueous components were exposed at an intensity of 200 μW/cm^2. Hydrogen peroxide evolution was measured in PBS with a selective hydrogen peroxide electrochemical probe (HP-250, Innovative Instruments, Inc.) driven by a potentiostat (EMstat2, Palm Sens) at 400 mV. Prior to each measurement, a calibration curve was generated using hydrogen peroxide standards. For the short term kinetic studies, triplicate hydrogels formed from 0.5-4 mg/mL aqueous components were exposed to 100, 200, 400, and 800 μW/cm^2 light intensities and measured every 10 min for 2 h. All characterization studies were conducted at room temperature.

For crosslinking dose studies, 4 mL of the prepolymer solution with a 4 mg/mL 2,6-AQS component was added to 60 mm dishes and photopolymerized with 150, 300, 600, 900, and 1,500 mJ/cm^2 energy using the low intensity 5 mW/cm^2 UVA source. A 3,000 mJ/cm^2 photopolymerizing exposure was performed using a high intensity 25 mW/cm^2 mercury arc lamp. The gels were allowed to stand for 20 min at room temperature and punched into 10 mm disks. Each gel was placed in its own container with 2 mL of DI water and placed in a shaker oscillating at 60 Hz at 37°C. The 2 mL extracts were saved and replaced at 2, 4, and 24 h. The 2,6-AQS content in the extract was measured by spectrophotometic absorption at 260 nm using a UV/Vis spectrophotometer (Evolution 600, Thermo Scientific) and calibrated to standards made from the 2,6-AQS stock solution. After 24 h of leaching, the hydrogels were then placed into a 48-well plate with 1 mL of DI water and exposed at 400 μW/cm^2 using the LED array. Hydrogen peroxide concentrations were measured after 2 h of exposure using the electrochemical probe as described. For the swelling ratio analysis, each gel was subsequently dried on a Kimwipe to remove unbound water and weighed. The hydrogels were then placed in a 65°C at least overnight and the change of weight was recorded.

2.4. Oxidative challenge experiments

For oxidative challenge experiments, TM-1 cells were prepared as described in the cell culture section in 24-well plates in 4 triplicate groups, with each well containing 1 mL of modified DMEM (mDMEM, specially formulated low glucose DMEM with pyruvate and without phenol red, riboflavin, and ferric nitrate, Invitrogen) and the appropriate hydrogel. The “light control” and “high ROS” groups were exposed at an intensity of 400 μW/cm^2 before light diffusion, the “low ROS” group was exposed at 100 μW/cm^2 before diffusion, and the “dark control” group was not exposed to light (LEDs were not given power). The groups were exposed for 4, 16, and 24 h in an incubator at 37°C supplemented with 5% CO_2. Viability of the triplicate sets were either analyzed by MTT or LIVE/DEAD viability staining. Hydrogen peroxide concentration in media was measured using the xylenol orange assay employed by Gülden, et al. [16]. Briefly, 10 μL of sample was placed in a 96 well plate with 140 μL of 25 mM H_2SO_4 to which 150 μL of a xylenol orange solution is added containing 0.5 mM $(NH_4)_2Fe(SO_4)_2$, 200 μM xylenol orange, and 200 mM sorbitol

dissolved in 25 mM H_2SO_4. The reaction was allowed to proceed for 45 min at room temperature which produced a stable colored solution whose absorbance was read at 570 nm by a plate reader (BioTek Synergy 4).

2.5. Statistical analysis

All data to be statistically analyzed were checked for normality by the Kolmogorov-Smirnov test ($p < 0.05$). Oxidative challenge data omitting the light control was analyzed by a nonparametric Kruskal-Wallis two-way ANOVA followed by a post-hoc analysis using Tukey's test. Pairwise comparisons of groups not requiring ANOVA were performed using the Mann-Whitney-Wilcoxon test. A Kruskal-Wallis one-way ANOVA using was performed on the bolus data to determine statistical significance.

3. Results and Discussion

3.1. Photoactive hydrogel fabrication and photoreduction mechanism

Photoactive hydrogels were fabricated by equal-volume mixtures of poly(ethylene glycol) diacrylate (PEG-DA) monomers and an aqueous 2,6-anthraquinone sulfonate (2,6-AQS, a water soluble AQ) solution, and were cast either into a mold to form a bulk hydrogel or between two glass substrates to form a thin film (Fig. 1). UV light exposure (at 365nm) over the prepolymer materials triggers two simultaneous reactions. (Fig. 1b). In one reaction, the 2,6-AQS molecules in the solution performs as a traditional photoinitiator by inducing radical polymerization. As 2,6-AQS is exposed to UV light, it first enters a singlet state and then quickly transitions to a triplet state through an intersystem crossing [26]. Once in this excited state, it abstracts a hydrogen with an electron from surrounding PEG-DA molecules, forming two radical species: a hydroxylated quinone (may be called ketyl radical of reduced anthraquinone) and a PEG-DA radical. As PEG-DA radicals accumulate, they react with the acrylated terminal groups of the monomer and proceed to crosslink into a network, forming a hydrogel [35]. The second reaction is a photografting/radical termination type reaction where the ketyl quinone radicals interact with existing radicals in the PEG polymers and form new, stable covalent bonds. The photografting mechanism of AQ compounds to a PEG matrix has been proposed by a recent work [36]. This reaction results in the reduction of one of the photoactive sites within the AQ moiety but allows for the other one to maintain its activity. The PEG networks rapidly polymerize under these conditions (typically < 30 s), forming hydrogels that were subsequently swollen and stored in DI water for later use.

Given that the reactions take place photocatalytically, the hydrogel material becomes intrinsically photopatternable. The prepolymer solution, with the maximum 2,6-AQS aqueous component (4 mg/mL, near solubility limit), is casted between a standard photomask with microscopic features and a glass cover slip that has been acrylated by silanization to anchor the resulting hydrogel. UV exposure from a 365 nm wavelength collimated light source photopolymerizes the material, followed by subsequent development in ethanol. Photo-crosslinked hydrogels were able to be reliably micropatterned down to a feature size of 2 μm (Fig. 2). This resolution limit is mainly due to the high concentration and rapid diffusivity of the photoinitiator in the prepolymer solution in the unsolidified film, resulting in soft edges [37]. Lithographic resolution could be potentially improved by

introducing a quencher that would limit radical diffusion within exposed regions [37]. The light-stimulated production of H_2O_2 from the micropatterned hydrogels_ENREF_38 was visualized using a fluorescent reporting system that employs horseradish peroxidase (HRP) as a catalyst to oxidize amplex red to its fluorescent form in the presence of hydrogen peroxide [38, 39] (Fig 2e).

3.2. Kinetic model and operating regimes

The kinetics of hydrogen peroxide production of the photoactive hydrogel is based on the mechanism by which AQs are able to catalytically generate ROS through a photoreduction process [26]. Similar to the photoinitiation reaction, the covalently bound AQ molecules are first excited to a singlet state that crosses into a highly reactive triplet state that can abstract a hydrogen atom from other molecules in its environment, forming an AQ ketyl radical. Unlike the photoinitiation condition, this AQ radical does not form covalent bonds with other radicals because it is unable to freely diffuse. If dissolved oxygen molecules are present, ground-state triplet oxygen reacts with the ketyl radical, abstracting the unpaired electron and yielding a superoxide anion ($\cdot O_2^-$) and a carbocation of AQS. Superoxide can then abstract the hydrogen from the hydroxyl group connected to the carbocation yielding a hydroperoxyl radical ($\cdot HO_2$) and a renewed AQS group that may repeat this cycle. Accumulated hydroperoxyl radicals then react with another of its species to form hydrogen peroxide and molecular oxygen. The details of this mechanism are much more complex than presented here and are described comprehensively elsewhere [26, 40]. A kinetic model to describe the generation of H_2O_2 based on this reaction mechanism is proposed in equation (1).

$$\frac{d[H_2O_2]}{dt} = k_g([AQ], [O_2], l, \lambda) - k_r[H_2O_2] \quad (1)$$

The reaction rate consists of a zeroth order generation term (k_g) and a first order loss or reverse reaction term (k_r). The generation rate constant k_g is a function of the AQ content within the hydrogel ([AQ]), the intensity (I) and wavelength (λ) of the light driving the reaction, and the local dissolved oxygen concentration ($[O_2]$). Higher generation rates are expected with increasing AQ and oxygen concentration within the gel as more catalytic centers and reactants would be present. The photoreduction cycling rate is expected to increase in response to higher light intensities and wavelengths that approach AQ's absorption maxima (typically between 300 and 400 nm for UVA band depending on the derivative and solvent [41]). The decay/reverse reaction first order constant k_r is an approximation that represents a composite of factors that would lead to breakdown or removal of H_2O_2 from the system, such as a possible reverse reaction with AQ, consumption by another chemical/biochemical reaction, reaction with the PEG matrix or vessel wall, spontaneous breakdown, or photolysis. As long as the chemical environment of the system is not significantly changing, k_r can be considered constant. Two regimes are predicted by this model. For relatively low concentrations of H_2O_2 ($k_g >> k_r[H_2O_2]$, Regime I), the rate of generation of hydrogen peroxide would be constant and result in a linear increase. However as concentrations increased, the generation rate would approach the decay rate ($k_g \sim k_r[H_2O_2]$, Regime II) and a steady state concentration of H_2O_2 would eventually result at a

value of k_g/k_r. These regimes allow one to provide either a constant generation of hydrogen peroxide to a system at low concentrations or a constant concentration of H_2O_2 that is actively maintained, both of which are tunable by 2,6-AQS concentration and light intensity, the latter of which can be done dynamically.

3.3. Kinetic analysis and parameter measurement

The hydrogen peroxide generation performance was determined by varying the concentration of 2,6-AQS in the prepolymer solution and the illuminating light intensity. A wavelength of 405 nm was selected for these studies to both reduce the effects of phototoxicity with *in vitro* experiments as well as improve user safety. First, the concentrations of H_2O_2 generated from Ø10 × 1.5 mm bulk hydrogel disks with 0.5 to 4 mg/mL 2,6-AQS aqueous prepolymer concentrations (all crosslinked with 365 nm UV at 150 mJ/cm^2) were measured. The photoactive hydrogels were then exposed to an LED array emitting 405 nm light at an intensity of 200 μW/cm^2 over a course of 20 days (Fig. 3a). The concentration of hydrogen peroxide generated by each hydrogel showed a transient increase in the first two hours, followed by reaching a steady-state value, with a magnitude that is positively correlated with 2,6-AQS prepolymer concentration. Moreover, the stability of the steady-state values were also functions of the initial 2,6-AQS concentration in the prepolymer, as the highest two tested concentrations lasted nearly 14 days before gradually decaying. The lower concentrations had a worse performance with 0.5 and 1 mg/mL decaying after 2 and 6 days, respectively.

Characteristics of both regimes described by the kinetic model were observable in measurements of hydrogen peroxide generated by irradiated hydrogels (Fig 3a). Early time points (< 1 h) show a linear increase in H_2O_2 concentration which indicate that the system was in Regime I. Under this condition the decay of H_2O_2 is considered negligible and the generation rate constant k_g can be approximated by taking the slope of a linear regression through the first 60 min of time points. After 1.5 h, the concentration profile became level and an equilibrium concentration of H_2O_2 is achieved and the conditions of Regime II are realized. The ratio of k_g/k_r was taken as the average equilibrium value of H_2O_2 before decay is observed.

Further investigation on the stability of ROS equilibrium in Regime II was conducted by placing a hydrogel under constant illumination of 405 nm light at 200 μW/cm^2, allowing it to generate hydrogen peroxide to a steady state level, and replacing the buffer (Fig. 3b). Subsequently, the H_2O_2 concentration was observed to quickly recover its original steady-state concentration, consistent with the continuous generation model described above. An important practical benefit of this equilibrium is that media changes, a common practice in cell culture and necessary for long-term oxidative challenge studies, would be possible without significantly disrupting the hydrogen peroxide levels.

The parameters k_g and k_r in the proposed kinetic model were determined by examining the hydrogen peroxide concentration profiles of photoactive hydrogels over 2 hours for a combined matrix of 2,6-AQS prepolymer concentrations and 405 nm light intensities at room temperature. Analysis of generation curves yielded values for H_2O_2 steady-state levels (k_g/k_r) and generation rates (k_g) for each gel/intensity combination (Fig. 3d, e). The

generation rate was converted to a mol rate of production by multiplying by the reaction (PBS) volume and represents the k_g for a 150 μL hydrogel volume. Both equilibrium and generation rate curves possessed similar trends, leveling off after a prepolymer concentration of 1 mg/mL but still showing increased activity with higher light intensities. The plateauing effect observed in these experiments was not simply due to light absorption through the hydrogel matrix as the thinner gel did not produce significantly different amounts of hydrogen peroxide in a normalized concentration and intensity scale. Therefore, this behavior could be potentially explained by saturation of binding sites for 2,6-AQS within the hydrogel matrix. This is consistent with the fact that increasing prepolymer 2,6-AQS concentration does not increase H_2O_2 production; however, higher light intensity would lead to increasing H_2O_2 production as the photochemical conversation can be further tuned with the light stimulation. These data show that the production of H_2O_2 is tunable over both 2,6-AQS concentration and light intensity, allowing them to act as independent adjustment parameters to deliver the desired dose.

The decay constant k_r was determined by dividing the equilibrium H_2O_2 concentration (k_g/k_r) by the molar generation rate and was found to be $15.5 \pm 1.92 \times 10^{-3}$ min^{-1} (mean ± standard deviation) over all concentration/intensity experiments. Decay due to light exposure was considered to be minimal, as the photolysis of H_2O_2 only begins to occur below 365 nm which is sufficiently far from the 405 nm source used [42]. Without light, it was found that it took 20 μM of H_2O_2 nearly 4 h to decompose in the presence of a photoactive PEG hydrogel (data not shown). Therefore, a majority of the loss of H_2O_2 is most likely due the existence of a reverse reaction under these conditions.

3.4. Material properties and leaching studies

According to the photosynthetic model proposed, the H_2O_2 generation capacity of these photoactive hydrogel matrices can be adjusted according to the level of 2,6-AQS integration and crosslinking density of the hydrogel by the exposure energy dose. Specifically, increased photo-exposure of the prepolymer solution should lead to increased integration of 2,6-AQS as well as generation of more polymeric crosslinks. To investigate the stability and retention of 2,6-AQS within the hydrogel matrix, we spectrophotometrically examined the aqueous extracts at 3 time points over 24 h of photoactive hydrogels polymerized with 150 to 3,000 mJ/cm^2 energy. The losses were determined over the 3 time points (Fig. 4a) and summed to determine the percentage loss as a function of crosslinking energy (Fig. 4b). Significant leaching of 2,6-AQS was observed for the lower energy doses but the losses drop precipitously with increasing energy. After extraction, these gels were then exposed to 405 nm light for 2 hours to determine their steady state concentrations (Fig. 4b). Increased crosslinking exposure energy resulted in a significantly higher H_2O_2 production. Consistent with our photografting model, these data show that increased crosslinking energy results in more 2,6-AQS integrating into the PEG backbone that also retain their photocatalytic capability. Subsequent to H_2O_2 generation tests, the weight of the hydrogels were measured before and after desiccation in an oven to determine their swelling ratios (Fig.4b). The swelling ratios, which were inversely proportional to the crosslinking density, decreased in an exponential fashion with increasing crosslinking energy. These results again support the photosynthetic model.

3.5. Oxidative challenge studies

To utilize the photoactive H_2O_2-producing material for generating *in vitro* oxidative stress, a two-component cell culture system has been devised in a standard 24-well format, which consisted of a lower plate that housed 405 nm LEDs with an adjustable power source and a stacked top plate containing cells surrounded by photoactive hydrogels (Fig. S1, see Supplemental Methods for description). In the top plate, TM-1 cells, a transformed human trabecular meshwork cell line, were first seeded in the center of each well at a density of 10,000 cells/well. Hydrogel rings were placed in wells around the cells such that oxygen diffusion and light microscopy were not impeded. Two control groups were used: a "light control" group that contained light-exposed non-photoactive hydrogels photopolymerized with Irgacure 2959 (I259, a non-cytotoxic [43] type I fragmenting photoinitiator with no residual photoactivity) and a "dark control" with a H_2O_2-producing hydrogel that is not exposed to light. Two experimental groups representing "low" and "high" generation rates were chosen empirically by adjusting the intensity of illumination of photoactive hydrogels containing 1 mg/mL 2,6-AQS to achieve a moderate and severe H_2O_2 dosage, which corresponded to generation rates of 260 and 350 nM/min. Early (4 h), mid (16 h), and late (24 h) oxidative challenge responses from 4 test groups using an methylthiazolyldiphenyl-tetrazolium bromide (MTT) assay [44] determined viability at each time point (Fig. 5a). All values were normalized to the dark controls and statistical analyses were performed to determine significance (see methods for details). Cells were stained with a combination of fluorescent calcein-AM and ethidium homodimer (LIVE/DEAD assay kit) corroborate the cell viability data (Fig. 5b). Initially, a media phototoxicity study was performed with TM-1 cells without hydrogels and it was found that serum-free modified DMEM (mDMEM) without riboflavin, ferric nitrate, and phenol red was necessary to maintain cell viability with 24 h exposure to 405 nm light (Fig. S2). Riboflavin has been well-established as a phototoxic agent in cell culture media [45-47]. As such, all cell experiments were conducted with mDMEM unless otherwise noted.

Statistical analyses demonstrated significant differences between groups and time points (both $p < 0.001$) and significant interaction between the values was found ($p < 0.05$). Cell viability in the dark and light control groups was found to be similar for all time points ($p > 0.10$) indicating that light exposure and the presence of the hydrogels in the culture media did not impact cell viability. The dark control demonstrated the lack of cytotoxicity of the system as the 2,6-AQS dye was safely retrained within the biologically inert [48] PEG hydrogel after initial leaching of unbound components (Fig. 4). No significant differences in viability were observed among the experimental groups at the 4 h time point compared to controls except for the high group ($p < 0.05$) and cells appeared to be morphologically normal under microscopy. However after 16 h, viability was reduced in the high (55%, $p < 0.001$) and low ROS (70%, $p < 0.01$) groups in comparison with control and additionally there was a significant difference between the experimental groups ($p < 0.05$). At 24 h, the MTT assay showed a further decrease in viability compared to the 16 h time point, as viability had been reduced to 40% and 60% compared to controls for the high and low ROS groups, respectively, and differed significantly from controls ($p < 0.001$) as well as each other ($p < 0.05$). A reduction in cell number was observed in the low ROS group, and very few viable cells remained in the high ROS group as seen by fluorescent staining. Cell death

by apoptosis, a known mode of death by oxidative stress [49], was confirmed by positive annexin V staining [50] at 16 h (Fig. S3).

One of the important features of this hydrogen peroxide generating system is that its kinetics can be adjusted by the independent manipulation of 2,6-AQS concentration and light intensity. To demonstrate that the tunability of the system also extends to biological results, we replicated the 24 h results of the low ROS group in the previous experiment by reducing the 2,6-AQS concentration of the hydrogel in half to 0.5 mg/mL and adjusted the light intensity to match the generation rate of 260 nM/min (using the standard curve from Fig. 3d). Indeed, the viability of the 0.5 mg/mL low ROS group was found to be very similar to the 1 mg/mL group (59% *vs* 64%, respectively; $p = 0.73$; Fig. S4).

Interestingly, no H_2O_2 concentrations were observed above the detection limit of 2 μM at any time in any group in the oxidative stress study. In addition, ROS generation experiments conducted analogously with the same groups but without cells also did not contain any detectable levels of H_2O_2 at any time point as well. Although the rate of generation of ROS was not high enough to result in accumulation of H_2O_2 in the media to detectable levels, the continual presentation of ROS leads to significant changes in cell viability.

As a comparison to the continuous exposure method, the viability of TM-1 cells was measured after delivering bolus doses of H_2O_2. Similar to the continuous exposure experiments, TM-1 cells were seeded in 24 well plates at 10,000 cells/well and given bolus doses of 5 to 500 μM of H_2O_2 in 1 mL of mDMEM and viability was determined 24 h later by the MTT assay (Fig. 5c). Overall viability, normalized to control (mDMEM only), was unaffected by even relatively high bolus doses of 500 μM H_2O_2 and was not found to be significantly different from control ($p = 0.168$). Similar experiments performed in Hank's buffered salt solution (HBSS) instead of mDMEM showed extremely high mortality rates above 5 μM boluses (data not shown), confirming that the TM-1 cells were unable to mount sufficient antioxidant defenses in media without nutrients needed to maintain long-term viability. The effect of the antioxidants on the oxidative profile were investigated by measuring the concentration of an initial 100 μM bolus of H_2O_2 over time in 1 mL of mDMEM with and without 10,000 cells/wells. The H_2O_2 concentration reduced exponentially at a first order rate with a decay constant of 0.143 ± 5.14% and 0.130 ± 3.12% min^{-1} with and without cells, respectively (least squares fit ± relative standard deviation, Fig. S5). The entire bolus dose was found to effectively dissipate after 30 min. The similarity of the decay constants suggests that the rate of H_2O_2 neutralization is cell independent while the concentration of antioxidants in the media, such as pyruvate [51], are high. This effect is likely responsible for the observed lack of apparent cell viability response to even relatively high bolus doses of H_2O_2 (Fig. 5c).

4. Conclusions

Photoactive PEG hydrogels produced by a single-step UV exposure were found to have micropatternable and well-behaved, predictable kinetic properties that could be used in conjunction with cell and protein patterning techniques [52-54] to provide predicable and tunable *in situ* generation of H_2O_2 on-demand by exposure to visible light. Hydrogen

peroxide generation rates and equilibrium concentrations were tunable by both the concentration of the photoactive 2,6-AQS component or dynamically by light intensity and were stable for up to 14 days of continuous exposure. These properties were exploited to provide continuous exposure of H_2O_2 to TM-1 cells at different rates that resulted in a dose response that had differing physiological consequences and outcomes. Interestingly, the 260 and 350 nM/min generation rates yielded an equivalent total ROS exposure a dosage of 230 and 500 μM over 24 h, respectively, yet these equivalent doses given acutely by bolus addition of H_2O_2 yielded very different biological results. These data show conclusively that a persistent low level of H_2O_2 had a more damaging effect on cells than an equivalent bolus dose of H_2O_2. The continuous H_2O_2 generating system described here provides a useful technique for continuously introducing ROS into cell culture media with the precision and stability that is difficult to obtain by more commonly used methods. Our approach allows one to not only allows the recreation of pathological conditions where tissues are under persistent redox imbalance but also assess what levels are relevant in the development and progression of disease. We speculate this technology can be exploited to significantly enhance the elucidation of molecular mechanisms of dysregulation and as a testing platform for evaluating treatments for diseases characterized by chronic oxidative stress.

Supplementary Material

Refer to Web version on PubMed Central for supplementary material.

Acknowledgments

This work was supported in part by NIH grants R01EY019475, R01EY019970, and P30EY12576. S.P.G. gratefully acknowledges support from NEI training grant T32EY15387-9. S.P.G. would like to thank Jingyuan Zhuo for helpful discussions of AQ photochemistry and assistance with spectrophotometry experiments, as well as Dr. Joshua T. Morgan for manuscript editing and discussions of oxidative stress.

References

[1]. Beckman KB, Ames BN. The Free Radical Theory of Aging Matures. Physiol Rev. 1998; 78:547–81. [PubMed: 9562038]

[2]. Berlett BS, Stadtman ER. Protein Oxidation in Aging, Disease, and Oxidative Stress. J Biol Chem. 1997; 272:20313–6. [PubMed: 9252331]

[3]. Cadenas E, Davies KJA. Mitochondrial free radical generation, oxidative stress, and aging. Free Radical Biol Med. 2000; 29:222–30. [PubMed: 11035250]

[4]. Liang F-Q, Godley BF. Oxidative stress-induced mitochondrial DNA damage in human retinal pigment epithelial cells: a possible mechanism for RPE aging and age-related macular degeneration. Exp Eye Res. 2003; 76:397–403. [PubMed: 12634104]

[5]. Seifried HE, Anderson DE, Fisher EI, Milner JA. A review of the interaction among dietary antioxidants and reactive oxygen species. J Nutr Biochem. 2007; 18:567–79. [PubMed: 17360173]

[6]. Thannickal VJ, Fanburg BL. Reactive oxygen species in cell signaling. Am J Physiol-Lung C. 2000; 279:L1005–L28.

[7]. Babior BM, Kipnes RS, Curnutte JT. Biological defense mechanisms. The production by leukocytes of superoxide, a potential bactericidal agent. J Clin Invest. 1973; 52:741. [PubMed: 4346473]

[8]. Ames BN, Cathcart R, Schwiers E, Hochstein P. Uric acid provides an antioxidant defense in humans against oxidant- and radical-caused aging and cancer: a hypothesis. Proc Natl Acad Sci. 1981; 78:6858–62. [PubMed: 6947260]

[9]. Gordillo GM, Sen CK. Revisiting the essential role of oxygen in wound healing. Am J Surg. 2003; 186:259–63. [PubMed: 12946829]

[10]. Aruoma O. Free radicals, oxidative stress, and antioxidants in human health and disease. J Am Oil Chem Soc. 1998; 75:199–212.

[11]. Catalá A. Lipid peroxidation of membrane phospholipids generates hydroxy-alkenals and oxidized phospholipids active in physiological and/or pathological conditions. Chem Phys Lipids. 2009; 157:1–11. [PubMed: 18977338]

[12]. Ishii H, Kurose I, Kato S. Pathogenesis of alcoholic liver disease with particular emphasis on oxidative stress. J Gastroenterol Hepatol. 1997; 12:S272–S82. [PubMed: 9407347]

[13]. Izzotti A, Bagnis A, Saccà SC. The role of oxidative stress in glaucoma. Mutat Res-Rev Mutat. 2006; 612:105–14.

[14]. Lebovitz RM, Zhang H, Vogel H, Cartwright J, Dionne L, Lu N, et al. Neurodegeneration, myocardial injury, and perinatal death in mitochondrial superoxide dismutase-deficient mice. Proc Natl Acad Sci. 1996; 93:9782–7. [PubMed: 8790408]

[15]. Gille J, Joenje H. Cell culture models for oxidative stress: superoxide and hydrogen peroxide versus normobaric hyperoxia. Mutat Res-DNAging. 1992; 275:405–14.

[16]. Gülden M, Jess A, Kammann J, Maser E, Seibert H. Cytotoxic potency of H2O2 in cell cultures: Impact of cell concentration and exposure time. Free Radical Biol Med. 2010; 49:1298–305. [PubMed: 20673847]

[17]. Chance B, Sies H, Boveris A. Hydroperoxide metabolism in mammalian organs. Physiol Rev. 1979; 59:527–605. [PubMed: 37532]

[18]. Barbouti A, Doulias P-T, Nousis L, Tenopoulou M, Galaris D. DNA damage and apoptosis in hydrogen peroxide-exposed Jurkat cells: bolus addition versus continuous generation of H2O2. Free Radical Biol Med. 2002; 33:691–702. [PubMed: 12208356]

[19]. Grune T, Reinheckel T, Joshi M, Davies KJ. Proteolysis in cultured liver epithelial cells during oxidative stress Role of the multicatalytic proteinase complex, proteasome. J Biol Chem. 1995; 270:2344–51. [PubMed: 7836468]

[20]. Antunes F, Cadenas E, Brunk U. Apoptosis induced by exposure to a low steady-state concentration of H2O2 is a consequence of lysosomal rupture. Biochem J. 2001; 356:549–55. [PubMed: 11368784]

[21]. Antunes F, Cadenas E. Cellular titration of apoptosis with steady state concentrations of H2O2: submicromolar levels of H2O2 induce apoptosis through Fenton chemistry independent of the cellular thiol state. Free Radic Biol Med. 2001; 30:1008. [PubMed: 11316581]

[22]. Kozlovsky N, Rudich A, Potashnik R, Bashan N. Reactive oxygen species activate glucose transport in L6 myotubes. Free Radical Biol Med. 1997; 23:859–69. [PubMed: 9378365]

[23]. Rudich A, Kozlovsky N, Potashnik R, Bashan N. Oxidant stress reduces insulin responsiveness in 3T3-L1 adipocytes. American Journal of Physiology-Endocrinology And Metabolism. 1997; 272:E935–E40.

[24]. Zweier JL, Duke SS, Kuppusamy P, Sylvester J, Gabrielson EW. Electron paramagnetic resonance evidence that cellular oxygen toxicity is caused by the generation of superoxide and hydroxyl free radicals. FEBS Lett. 1989; 252:12–6. [PubMed: 2547649]

[25]. Goor, G.; Glenneberg, J.; Jacobi, S. Hydrogen Peroxide. Ullmann's Encyclopedia of Industrial Chemistry. Wiley-VCH Verlag GmbH & Co. KGaA; 2000. p. 393-427.

[26]. Görner H. Photoreduction of 9, 10 - Anthraquinone Derivatives: Transient Spectroscopy and Effects of Alcohols and Amines on Reactivity in Solution. Photochem Photobiol. 2003; 77:171–9. [PubMed: 12785056]

[27]. Koch T, Jacobsen N, Fensholdt J, Boas U, Fenger M, Jakobsen MH. Photochemical Immobilization of Anthraquinone Conjugated Oligonucleotides and PCR Amplicons on Solid Surfaces. Bioconj Chem. 2000; 11:474–83.

[28]. Geuskens G, Etoc A, Di Michele P. Surface modification of polymers VII.: Photochemical grafting of acrylamide and N-isopropylacrylamide onto polyethylene initiated by anthraquinone-2-sulfonate adsorbed at the surface of the polymer. Euro Polym J. 2000; 36:265–71.

[29]. Liu J, Sun G. The synthesis of novel cationic anthraquinone dyes with high potent antimicrobial activity. Dyes Pigments. 2008; 77:380–6.

[30]. Liu N, Sun G, Zhu J. Photo-induced self-cleaning functions on 2-anthraquinone carboxylic acid treated cotton fabrics. J Mater Chem. 2011; 21:15383–90.

[31]. Bilyk A, Li S, Murphy J, Petinakis S, Zerdin K, Scully A. Photoactive nanocoating for controlling microbial proliferation on polymeric surfaces. Prog Org Coat. 2008; 62:40–8.

[32]. Zerdin K, Horsham MA, Durham R, Wormell P, Scully AD. Photodynamic inactivation of bacterial spores on the surface of a photoactive polymer. React Funct Polym. 2009; 69:821–7.

[33]. Catalina F, Peinado C, Blanco M, Corrales T, Allen NS. Synthesis, photochemical and photoinitiation activity of water-soluble copolymers with anthraquinone chromophores as side-chain groups. Polymer. 2001; 42:1825–32.

[34]. Foyle VP, Takahashi Y, Guillet JE. Photocatalytic production of hydrogen peroxide using polymer bound anthraquinone. I. Photoproducts in 2 - hydroxyethyl methacrylate hydrogels swollen with water and 2 - propanol. J Polym Sci Pol Chem. 1992; 30:257–69.

[35]. Ifkovits JL, Burdick JA. Review: photopolymerizable and degradable biomaterials for tissue engineering applications. Tissue Eng. 2007; 13:2369–85. [PubMed: 17658993]

[36]. Tsaplev YB. Photochemical transformations of anthraquinone in polymeric alcohols. Russ J Phys Chem A. 2012; 86:1909–14.

[37]. Takada K, Sun H-B, Kawata S. Improved spatial resolution and surface roughness in photopolymerization-based laser nanowriting. Appl Phys Lett. 2005; 86:071122–3.

[38]. Zhou M, Diwu Z, Panchuk-Voloshina N, Haugland RP. A Stable Nonfluorescent Derivative of Resorufin for the Fluorometric Determination of Trace Hydrogen Peroxide: Applications in Detecting the Activity of Phagocyte NADPH Oxidase and Other Oxidases. Anal Biochem. 1997; 253:162–8. [PubMed: 9367498]

[39]. Lee JY, Shah SS, Yan J, Howland MC, Parikh AN, Pan T, et al. Integrating sensing hydrogel microstructures into micropatterned hepatocellular cocultures. Langmuir. 2009; 25:3880–6. [PubMed: 19275186]

[40]. Liu N, Sun G. Production of reactive oxygen species by photoactive anthraquinone compounds and their applications in wastewater treatment. Ind Eng Chem Res. 2011; 50:5326–33.

[41]. Alegría AE, Ferrer A, Santiago G, Sepúlveda E, Flores W. Photochemistry of water-soluble quinones. Production of the hydroxyl radical, singlet oxygen and the superoxide ion. J Photochem Photobiol A: Chem. 1999; 127:57–65.

[42]. Baxendale J, Wilson J. The photolysis of hydrogen peroxide at high light intensities. J Chem Soc, Faraday Trans. 1957; 53:344–56.

[43]. Williams CG, Malik AN, Kim TK, Manson PN, Elisseeff JH. Variable cytocompatibility of six cell lines with photoinitiators used for polymerizing hydrogels and cell encapsulation. Biomaterials. 2005; 26:1211–8. [PubMed: 15475050]

[44]. Sylvester P. Optimization of the Tetrazolium Dye (MTT) Colorimetric Assay for Cellular Growth and Viability. Drug Design Discov. 2011; 716:157–68.

[45]. Grzelak A, Rychlik B, Bartosz G. Light-dependent generation of reactive oxygen species in cell culture media. Free Radical Biol Med. 2001; 30:1418–25. [PubMed: 11390187]

[46]. Sato K, Taguchi H, Maeda T, Minami H, Asada Y, Watanabe Y, et al. The primary cytotoxicity in ultraviolet-a-irradiated riboflavin solution is derived from hydrogen peroxide. J Invest Dermatol. 1995; 105:608–12. [PubMed: 7561167]

[47]. Edwards A, Silva E, Jofré B, Becker M, De Ioannes A. Visible light effects on tumoral cells in a culture medium enriched with tryptophan and riboflavin. J Photochem Photobiol B: Biol. 1994; 24:179–86.

[48]. Krsko P, Libera M. Biointeractive hydrogels. Materials today. 2005; 8:36–44.

[49]. Chandra J, Samali A, Orrenius S. Triggering and modulation of apoptosis by oxidative stress. Free Radical Biol Med. 2000; 29:323–33. [PubMed: 11035261]

[50]. Vermes I, Haanen C, Steffens-Nakken H, Reutellingsperger C. A novel assay for apoptosis flow cytometric detection of phosphatidylserine expression on early apoptotic cells using fluorescein labelled annexin V. J Immunol Methods. 1995; 184:39–51. [PubMed: 7622868]

[51]. Giandomenico AR, Cerniglia GE, Biaglow JE, Stevens CW, Koch CJ. The Importance of Sodium Pyruvate in Assessing Damage Produced by Hydrogen Peroxide. Free Radical Biol Med. 1997; 23:426–34. [PubMed: 9214579]

[52]. Zhao S, Chen A, Revzin A, Pan T. Stereomask lithography (SML): a universal multi-object micro-patterning technique for biological applications. Lab Chip. 2011; 11:224–30. [PubMed: 21113523]

[53]. Xing S, Zhao S, Pan T. Print-to-print: a facile multi-object micro-patterning technique. Biomed Microdevices. 2012:1–8.

[54]. Ding Y, Huang E, Lam KS, Pan T. Microfluidic impact printer with interchangeable cartridges for versatile non-contact multiplexed micropatterning. Lab Chip. 2013

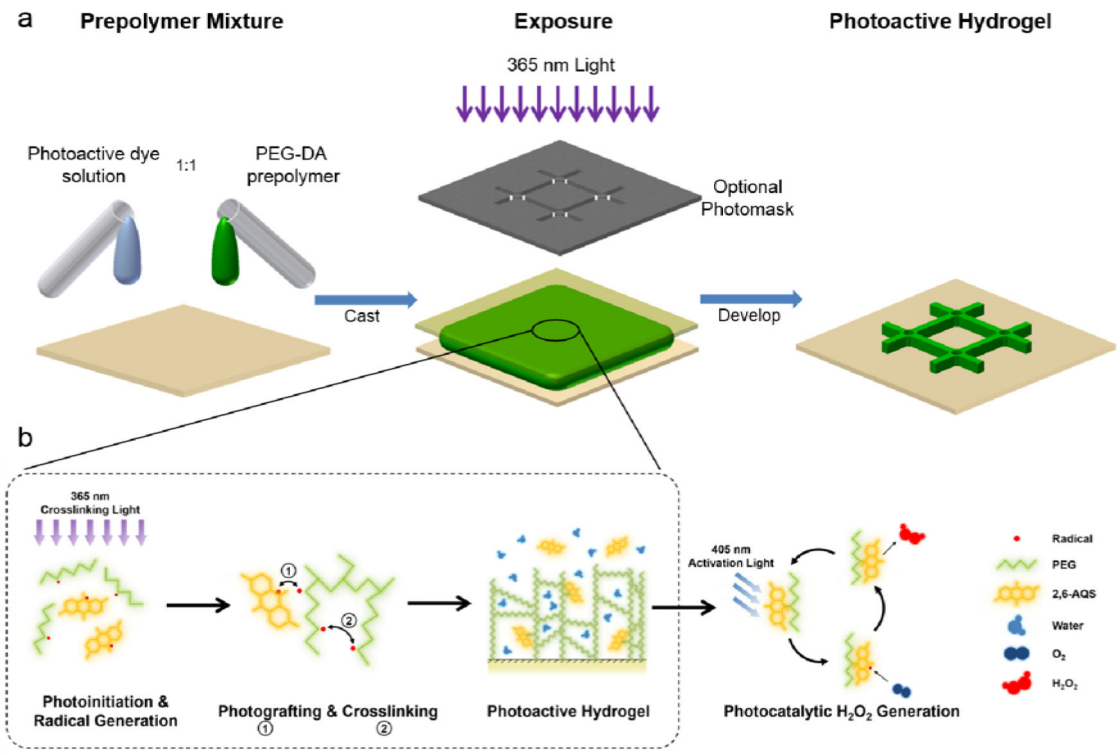

Fig. 1.

Process flow and photochemical reactions. (a) Process flow diagram. An equivolume mixture of aqueous AQS solutions and PEG-DA are casted over a substrate and photolithographically patterned with UV light. The resulting structures can be developed with water and activated with 405 nm light. (b) Chemical reaction diagram of the 2-in-1 synthesis method that yields both a crosslinked hydrogel and photografted AQS catalytic centers that yield hydrogen peroxide upon exposure to 405 nm light.

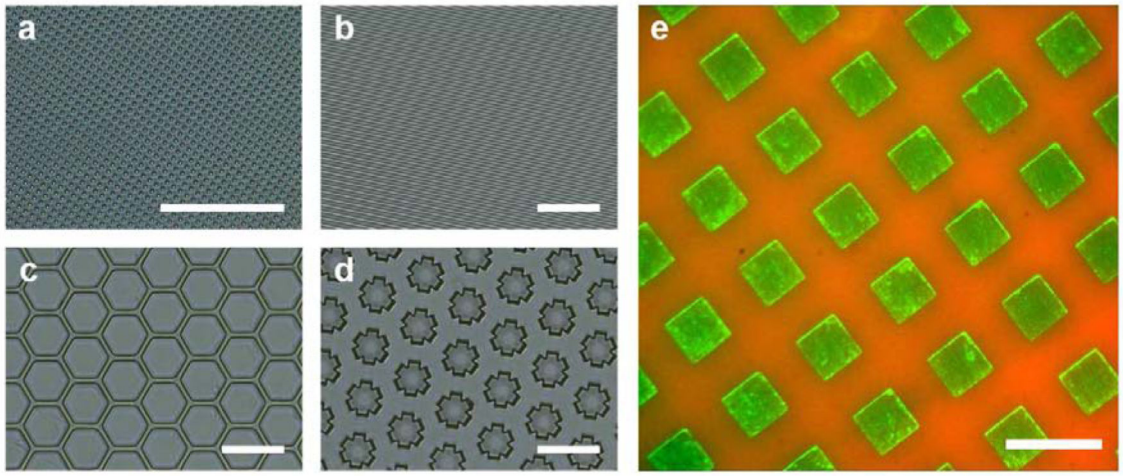

Fig. 2.

Photopatterning of photoactive hydrogels. Brightfield micrographs of patterned hydrogels with (a) 2, (b) 5, (c) 10, and (d) 25 μm features. (e) Fluorescent micrograph of amplex red (red) activated by the generation of hydrogen peroxide from a 5 min UV exposure of 50 μm photoactive hydrogel pillars (green). Scalebars = 100 μm.

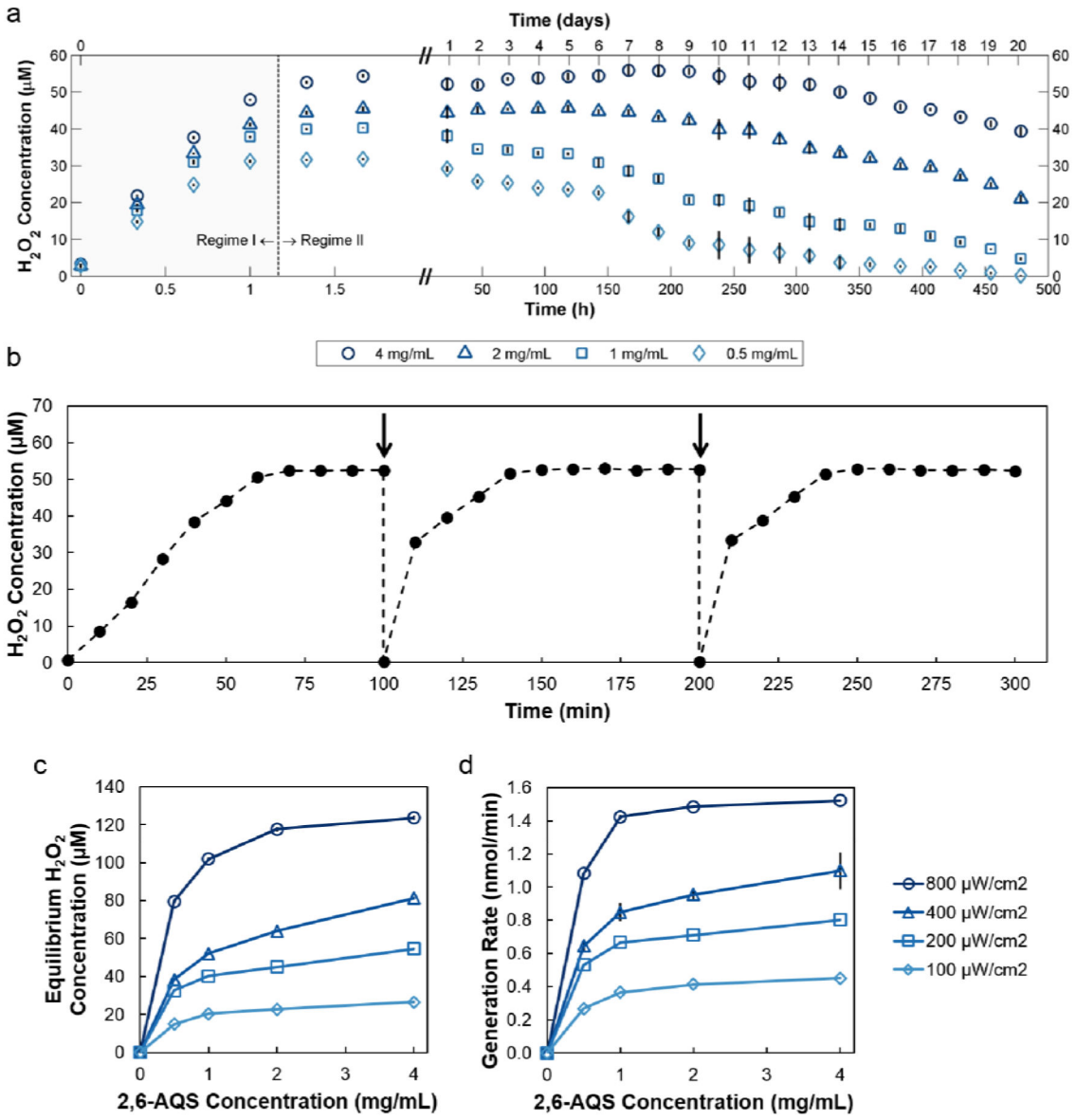

Fig. 3.

Hydrogen peroxide generation profiles and kinetic data. (a) Long term generation of hydrogen peroxide from Ø10×1.5 mm photoactive hydrogel discs of different 2,6-AQS concentrations exposed to 405 nm light continuously over 20 days. (b) Restoration of equilibrium concentrations of hydrogen peroxide under constant illumination after buffer exchange indicated by the arrows. (c) Equilibrium concentrations and (d) generation rates of hydrogen peroxide from hydrogels formulated with different 2,6-AQS concentrations and illumination intensities of 405 nm light. Error bars indicate standard deviation (n = 3). All studies were conducted in 1 mL PBS.

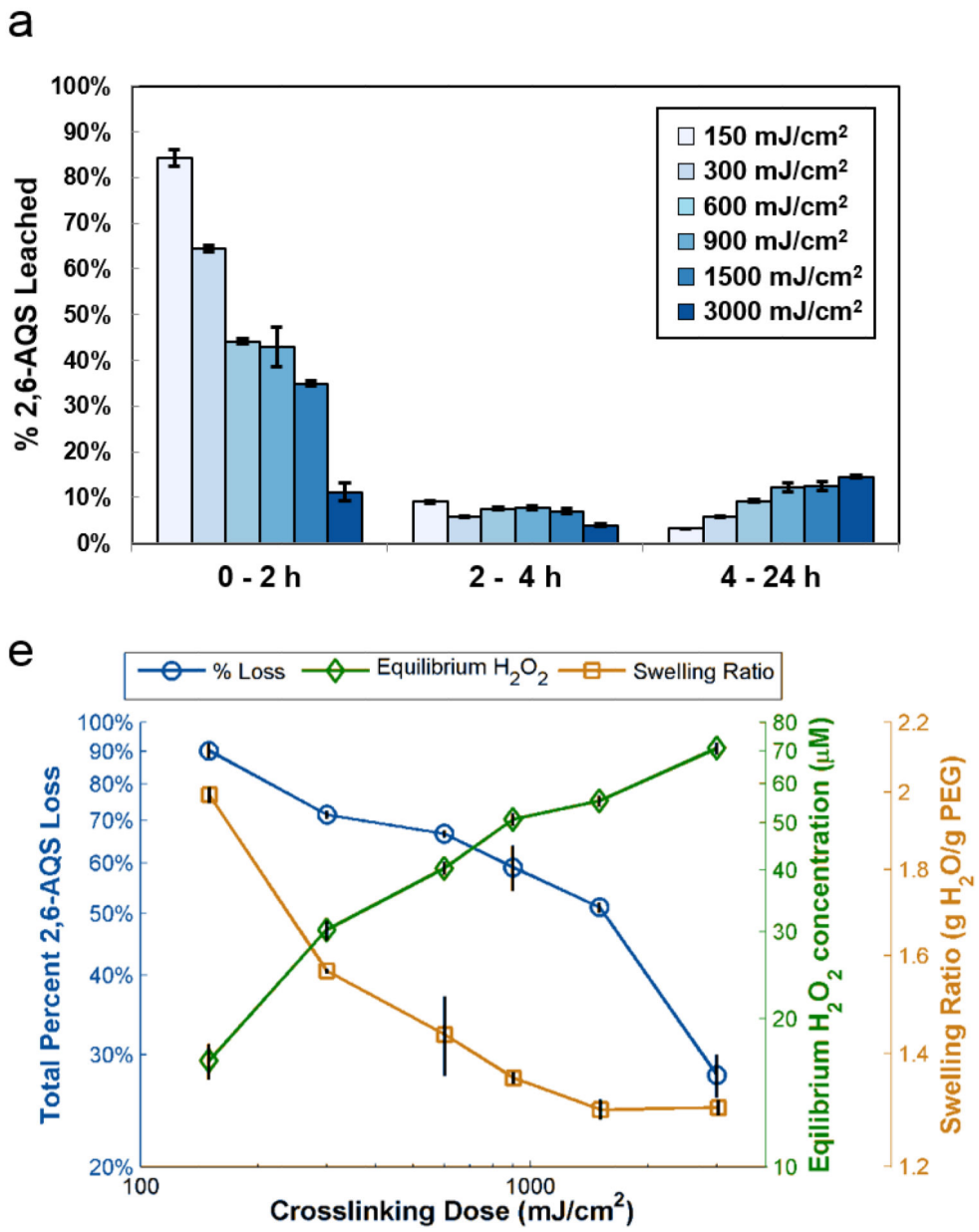

Fig. 4.

Effect of crosslinking dose on the stability and photocatalytic activity of AQS in hydrogels. (a) Loss of 2,6-AQS from hydrogels crosslinked with different exposure intensities measured over 24 h by spectrophotometry at 260 nm. Fresh DI water was replaced between intervals. (b) Comparison of hydrogel properties as a function of crosslinking dose. The cumulative loss of leeched 2,6-AQS from hydrogels in A showing retention with increasing dose. The subsequent equilibrium H_2O_2 concentration generated from leached hydrogels after 2 h of exposure of 405 nm light at 200 μW/cm^2 demonstrating that retained 2,6-AQS moieties are photoactive. Lastly, the swelling ratios of leached photoactive hydrogels with crosslinking dose are shown indicating increased matrix density with crosslinking dose. All hydrogels were made with a 4 mg/mL 2,6-AQS solution. Error bars indicate standard deviations (n = 3).

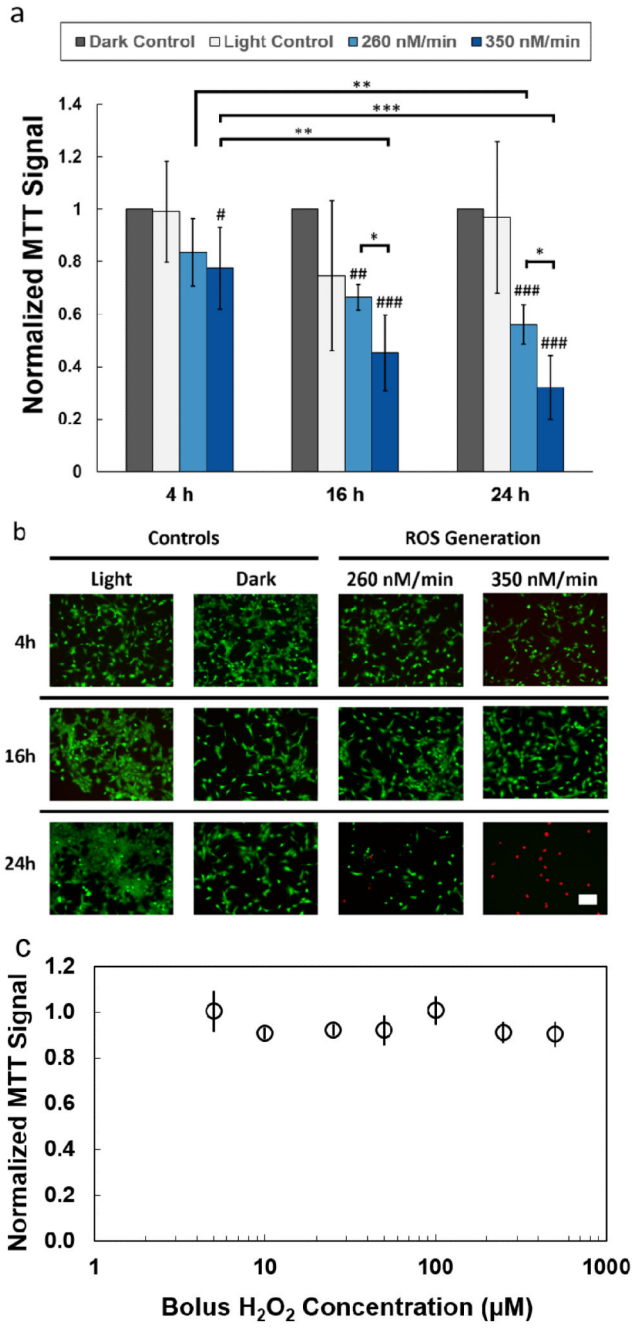

Fig. 5.

Oxidative challenge study. (a) Viability quantified by MTT normalized to the dark control at 4, 16, and 24 h of continuous oxidative stress. See text for discussion of groups. (b) Fluorescent micrographs of LIVE/DEAD stained samples of the groups and time points in A with viable cells in green and dead cells in red. (c) Viability quantified by MTT of 5 – 500 μM H_2O_2 bolus doses after 24 h in mDMEM. All studies were performed with TM-1 cells at a 10k/well in 1 mL of media. Error bars indicate standard deviations (n = 3). Symbols: # indicate significance to the dark control at that time point; * indicate significance between indicated groups. #/* = $p < 0.05$; ##/** = $p < 0.01$; ###/*** = $p < 0.001$. Scalebar = 100 μm.